Molecular Therapy
Methods & Clinical Development
Original Article

Selective RNAi silencing of Schwann cell Piezo1 alleviates mechanical hypersensitization following peripheral nerve injury

Brandon Itson-Zoske,[1] Uarda Gani,[1] Alexander Mikesell,[2] Chensheng Qiu,[1,3] Fan Fan,[4] Cheryl L. Stucky,[2] Quinn H. Hogan,[1] Seung Min Shin,[1] and Hongwei Yu[1]

[1]Department of Anesthesiology, Medical College of Wisconsin, Milwaukee, WI 53226, USA; [2]Department of Cell Biology, Neurobiology, and Anatomy, Medical College of Wisconsin, Milwaukee, WI 53226, USA; [3]Department of Orthopedic Surgery, Affiliated Hospital of Qingdao University, Qingdao 266000, China; [4]Department of Physiology, Medical College of Georgia, Augusta University, Augusta, GA 30912, USA

The present study was designed to investigate the role of Schwann cell (SC) Piezo1 in peripheral nociception. We first developed an AAV vector that has primary SC tropism after delivery into the sciatic (or tibial) nerve. This was achieved by packing AAV-GFP transcribed by a CBA promoter using a capsid AAVolig001 to generate AAVolig001-CBA-GFP. Six weeks after intraneural injection of AAVolig001-CBA-GFP in naive rats, GFP expression was detected selectively in both myelinating SCs (mSCs) and non-myelinating SCs (nmSCs). A dual promoter and bidirectional AAV encoding a U6-driven short hairpin RNA against rat Piezo1 (PZ1shRNA) and CBA-transcribed GFP was packed with capsid olig001 (AAVolig001-PZ1shRNA), and AAV was injected into unilateral sciatic (or tibial) nerve immediately after induction of common peroneal nerve injury (CPNI). Results showed that the development of mechanical hypersensitivity in the CPNI rats injected with AAVolig001-PZ1shRNA was mitigated compared to rats subjected to AAVolig001-scramble. Selective *in vivo* SC transduction and functional block of Piezo1 channel activity of primary cultured SCs was confirmed. These data demonstrate that (1) AAVolig001 has unique and selective primary tropism to SCs via intraneural delivery, and (2) SC Piezo1 contributes to mechanical hypersensitivity following nerve injury.

INTRODUCTION

Schwann cells (SCs), the specialized glial cells of the peripheral nervous system (PNS), are critical for the function and health of the PNS. Although exploration of the pathogenesis underlying neuropathic pain has centered on neuronal mechanisms, accumulating evidence suggests that SCs, which are physiologically exposed to mechanical stresses and detect nerve injury, play important roles in the development and maintenance of neuropathic pain.[1–6]

Piezo channels, including Piezo1 and Piezo2, are mechanosensitive channels that are expressed widely throughout the body of mammals.[7,8] Sensory neuronal Piezo2 contributes to peripheral mechanical sensitization,[9] while sensory neuron-resided Piezo1 is reported to transduce mechanical itch but not nociception.[10] Seminal studies propose that Piezo1 is a polymodal sensor of diverse mechanical forces primarily expressed in non-sensory tissues, playing essential roles in a wide range of physiological processes in multiple organs and systems[11] and likely participating in other biological functions yet to be discovered. Recent studies found enriched Piezo1 (and Piezo2) expression in SCs,[12] and SCs are required for mechanosensation,[13] suggesting that Piezo1 may participate in the mechanosensation of SCs. One study used a classic Cre-Loxp strategy via a myelin protein zero (MPZ) promoter transcribing Cre for conditional Piezo1 or -2 ablations in myelinating SCs (mSCs), showing that Piezo1 inhibits myelination, while Piezo2 facilitates myelin formation in the PNS.[12] We reported the identification of enriched Piezo1 expression in rat SCs, including mSCs and non-mSCs (nmSCs), and SCs-Piezo1 is more sensitive, compared to sensory neurons and other non-neuronal cells in the PNS, to Piezo1 agonist Yoda1 stimulation that induces mechanical hypersensitivity when applied into the sciatic nerve in rats.[14] This implies that SCs-Piezo1 activation may contribute to the enhanced mechanical nociception.

This study aims to investigate whether the adeno-associated virus (AAV)-mediated RNAi approach can be utilized to study the role of SCs-Piezo1 in peripheral nerves. We characterized the tropism and transduction efficiency of a novel "oligotrophic" AAV capsid called olig001, which is generated using capsid shuffling and directed evolution after rat intravenous delivery and subsequent capsid clone rescue, showing a >95% tropism for oligodendrocytes after rat intracranial infusion.[15,16] This oligodendrocyte-specific AAV capsid is in clinical testing for *in vivo* gene supplementation therapy for Canavan

Received 18 September 2024; accepted 7 February 2025;
https://doi.org/10.1016/j.omtm.2025.101433.

Correspondence: Seung Min Shin, Department of Anesthesiology, Medical College of Wisconsin, Milwaukee, WI 53226, USA.
E-mail: smshin@mcw.edu
Correspondence: Hongwei Yu, Department of Anesthesiology, Medical College of Wisconsin, Milwaukee, WI 53226, USA.
E-mail: hyu@mcw.edu

disease.[17] We hypothesize that AAVolig001 may also determine primary tropism to the SCs when delivered into the sciatic nerve.

We first generated AAVolig001-GFP transcribed by a constitutive chicken β-actin (CBA) promoter, which was injected into the adult rat peripheral nerve. After injection, immunohistochemistry (IHC) revealed GFP expression selectively in both mSCs and nmSCs, but not in afferent axons and somata of sensory neurons in the dorsal root ganglia (DRG). We next designed a dual promoter and bidirectional AAV construct encoding a U6-driven PZ1shRNA (Piezo1-short hairpin RNA) and CBA-transcribed GFP scramble (Sc) reporter, and this construct was packed into capsid olig001 to generate AAVolig001-PZ1shRNA. *In vivo* test by intraneural delivery showed that AAVolig001-PZ1shRNA-mediated selective silencing of SCs-Piezo1 mitigates the development of mechanical hypersensitization, while the thermal hypersensitization is spared in rats with common peroneal nerve injury (CPNI)-induced neuropathic pain. RNAi silencing of Piezo1 via intraneural delivery of AAVolig001-PZ1shRNA provides a rapid and selective approach for investigating the roles of SCs-Piezo1 in peripheral nerve mechanobiology.

RESULTS

AAVolig001 determines primary SC tropism after sciatic nerve delivery

Prior studies demonstrate that AAV packed by a novel oligotropic capsid olig001 shows >95% oligodendrocyte transduction after delivery into the rat brain.[15] We, therefore, tested whether AAVolig001 encoding GFP by a constitutive poly II promotor CBA (AAVolig001-GFP) has primary SC tropism after intrasciatic delivery. We injected AAVolig001-GFP in a dose of 4×10^{11} GC viral particles (20 μL) per animal into the right sciatic nerve of adult rats. The dose was determined according to the results of a brief dose-ranging test using 1×10^{11} GC viral particles applied in 5 or 20 μL (two rats per 5 and 20ul injection) in the pilot study for which we found less efficacy of transgene expression at a lower dose (data not shown). Five weeks after injection of 4×10^{11} GC viral particles into the sciatic nerve, the animals were euthanized, tissue was harvested, and GFP expression in the ipsilateral L3–L5 DRG (and contralateral ones), sciatic nerve and its three terminal branches, lumber spinal cord, and hindpaw skin was analyzed by IHC.

IHC revealed GFP expression in the sciatic nerves of all rats (10) injected with AAVolig001-GFP. In the sciatic nerve and its terminal branches, GFP signals exhibiting SC profile were detected in the nerve fascicles that accounted for ∼50% of the cross-sectional area of the sciatic nerve (the ages of the rats when tissues harvested were ∼4 months old). Four out of 10 rats showed higher GFP signals in the larger-diameter fascicles than in the small-diameter fascicles, and other injections showed detection of comparable GFP signals in both large and small nerve fascicles (Figures 1A–1B1). GFP signals were identified in the tibial and sural nerves (Figures 1C and 1D) but were low in the common peroneal nerve (data not shown). In the DRG, spinal cord, and hindpaw glabrous skin, no apparent GFP^+ sensory neurons and glia or spinal cord neurons and neuropils in the dorsal and ventral horn or glial cells and skin were observed (Figures S1A–S1C). Results suggest an *in vivo* restricted biodistribution of AAVolig001-GFP within the sciatic nerve and its branches after sciatic nerve vector delivery.

Colabeling of GFP with SC markers and neuronal markers showed that GFP^+ cells exhibited the typical SC pattern, indicating AAVolig001 induction of GFP efficient and selective transduction in the SCs. No GFP signals were colocalized with the sensory neuronal markers that labeled large and small afferent fibers (Figures 1C–1J). The cross-sectional IHC images of GFP and MPZ (a marker of mSCs) coimmunostaining were used to quantitatively assess *in vivo* mSC transduction by a method as shown in Figure S2, since an mSC myelinates a single large diameter axon forming a single myelin sheath.[18,19] *In vivo* transduction rate (three rats), calculated as the GFP-labeled SCs (average 2,124) out of the total MPZ^+ mSCs (average 4,256) in larger-diameter nerve fascicles, is ∼50% (30%–64%). AAVolig001-expressed GFP signals were also overlaid on P75NTR and GAP43, which are highly expressed in nmSCs,[20–22] indicating the tropism of AAVolig001 to nmSCs. However, estimation of the transduction rate in nmSCs is difficult since an nmSC, also called Remak SC, enfolds or accommodates multiple small-diameter non- or less-myelinated axons, forming Remak bundles.[23,24] We, therefore, counted the percentage of $P75NTR^+$ small fibers that were wrapped by GFP^+ SCs, representative of an estimation of AAVolig001 tropism to nmSCs. Results showed that 40%–80% of $P75NTR^+$ small fibers were ensheathed by GFP^+ SCs. These results revealed that intrasciatic delivery of AAVolig001-GFP induced selective and efficient transduction to both mSCs and nmSCs.

For comparison, we injected AAV6-CBA-GFP in a comparable dose of 4×10^{11} GC particles (20 μL) into the sciatic nerve of naive rats. IHC of GFP expression 5 weeks after injection of AAV6-CBA-GFP showed extensive GFP detection in SCs, afferent axons, sensory neuronal somata (L3–L5), neuropil in the lumbar spinal dorsal horn, and motor neurons in the spinal ventral horn (Figure 2). These results demonstrate that although both AAVolig001 and AAV6 (both using the CBA promoter) efficiently transduce SCs via intrasciatic delivery, AAVolig001 has unique and selective primary tropism to the SCs in the sciatic nerve, and AAVolig001 determines the SC tropism without the need to incorporate SC-specific elements, such as a SC-specific promoter.

Cell-based knockout/knockdown validates the specificity of Piezo1 antibody

We used a rabbit Piezo1 antibody in our previous study.[14] This study used a mouse Piezo1 antibody, which is an affinity chromatography purified mouse monoclonal antibody (isotope IgG2a) raised against recombinant protein encompassing amino acids 1,275–1,540 of human Piezo1 (NBP2-75617, Novus Biologicals, Centennial, CO). The antibody has been validated in its specificity and used to detect Piezo1 expression by immunoblots, immunocytochemistry (ICC), and IHC of rodent and human samples in previous studies.[25,26] We further validated the specificity of this mouse Piezo1 monoclonal antibody

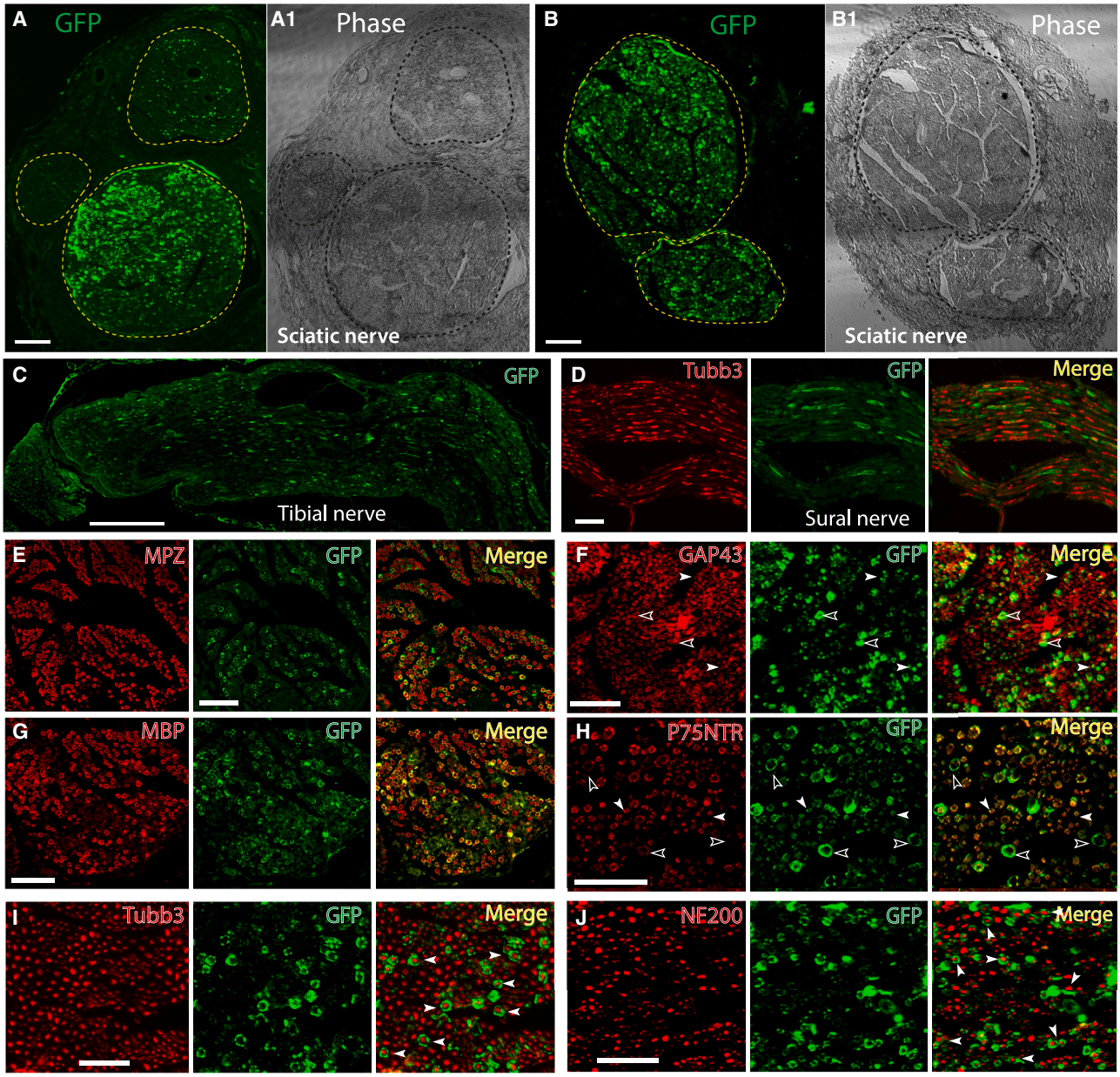

Figure 1. GFP expression after intrasciatic AAVolig001-CBA-GFP

(A–D) GFP expression in the nerve fascicles (dashed circles) of cross-sectioned sciatic nerves (A and B). Detection of GFP signals in longitudinal sections of tibial and sural serves (C and D). (E–J) Representative IHC images illustrate selective GFP expression in both mSCs and nmSCs, colabeled with SCs markers MPZ, MBP, GAP43, and P75NTR (E–H). Empty and white arrowheads in (F) and (H) point to mSCs and nmSCs, respectively; no GFP signals in the afferent axons labeled by Tubb3 and NF200 (I and J). Scale bars (μm): (A) and (B), 100; (C), 500; (D)–(F), 100. Antibodies for double labeling are indicated in each montage IHC image. Scales: 50 μm for all. GAP43, growth-associated protein 43; MBP, myelin basic protein; MPZ, myelin protein zero; NF200, neurofilament 200; P75NTR, p75 neurotrophin receptor; and Tubb3, β3-tubulin.

to detect Piezo1 by a CRISPR-Cas9 genome editing approach using N2A cells' stable expression of Cas9, as described previously.[14] Results showed that the antibody recognized a clean ∼300-kDa band predicted as the canonical Piezo1 protein by immunoblot, with comparable band density in the control N2ACas9 cells and N2ACas9 cells expressing mCherry, while lentivector-mediated Piezo1-guide RNA (gRNA) expression in N2ACas9 cells induced complete ablation of Piezo1 protein expression. We further validate the immunostaining specificity of Piezo1 antibody by ICC. Results also showed that Piezo1 immunoreactivity vanished in the N2ACas9 cells with lentivector-mediated Piezo1-gRNA expression, compared to controls (Figures 3A–3C). These data verify the

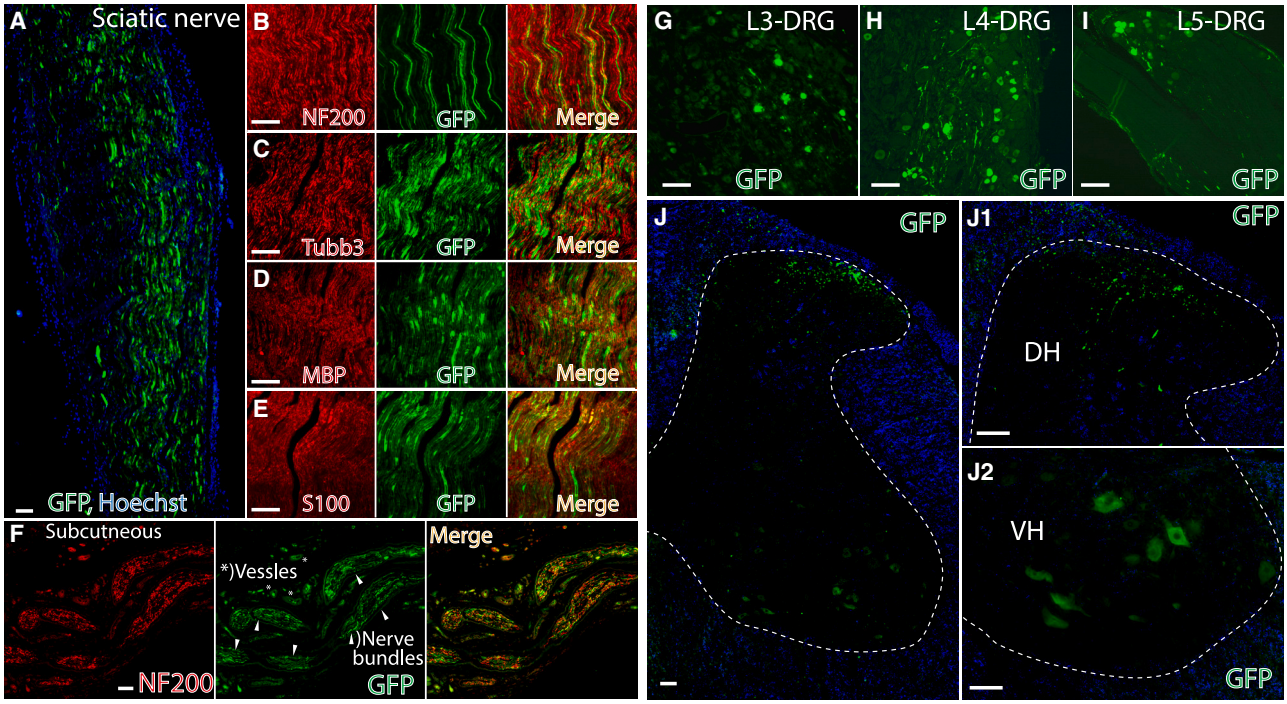

Figure 2. Non-cellular selective transduction after sciatic nerve delivery of AAV6-CBA-GFP

(A–F) Representative IHC images illustrate that 5 weeks after sciatic nerve injection of AAV6-CBA-GFP, GFP signals are detected in the afferent axons and SCs of the sciatic nerve by double labeling of GFP with neuronal markers (Tubb3 and NF200) and SC markers (MBP and S100). (F) Representative IHC images show GFP signal detection, colabeled with NF200 in the sensory terminals on the subcutaneous section. (G–I) Neuronal profile of GFP signals in the L3, L4, and L5 DRG ipsilateral to injection. (J–J2) GFP signals are also detected in the spinal cord dorsal horn (DH) neuropil and ventral horn (VH) motor neurons. Scale bars: 50 μm for all.

specificity of this monoclonal antibody in the detection of Piezo1 expression by immunoblot and immunostaining.

We designed a dual promoter and bidirectional AAV expression plasmid in which U6 promoter drives PZ1shRNA and CBA promoter transcribes GFP Sc, respectively. Two PZ1shRNAs were constructed and tested in cell-based *in vitro* tests using NG108 neuronal cells. The results revealed that PZ1shRNA1 induced >85% reduction of Piezo1 protein level after transfection into neuronal-like NG108 cells, compared with the sham- and Sc control-transfected cells (Figures 3D and 3E). Functional Piezo1 knockdown was verified since Yoda1-evoked increase of intracellular calcium (Ca_i^{2+}) in the PZ1shRNA1 expressing NG108 cells was significantly reduced (Figures 3F and 3G). PZ1shRNA1 was used to produce AAVolig001-PZ1shRNA for *in vivo* test.

Sciatic nerve injection of AAVolig001-PZ1shRNA partially reduces nerve injury-induced mechanosensitization

We next tested whether *in vivo* RNAi silencing of Piezo1 selectively in the SCs will affect hindpaw hypersensitivity after peripheral nerve injury in rats. We used a CPNI model. Commonly used neuropathic pain models are ligation and transection of the tibial nerve injury (TNI) or Spared nerve injury (SNI), but these two models often show both abnormal sensory function and loss of motor function, and assessment of the sensory system could be affected by motor defects.[27] The common peroneal nerve is the smaller and terminal branch of the sciatic nerve, and ligation of the common peroneal nerve was reported with long-lasting behavioral allodynia and thermal hyperalgesia but intact motor functions.[27,28] Additionally, AAVoligo001, after sciatic nerve injection, shows preferable biodistribution along the tibial nerve because high SC transduction in the tibial nerve was observed more than that in common peroneal and sural nerves after AAVolig001 sciatic nerve injection; this may induce more biological effects of SCs-Piezo1 silencing since injured terminal nociceptive territories can be re-innervated or hyperinnervated by uninjured fibers.[29–32]

We first evaluated sensory behaviors in naive rats after sciatic nerve injection of AAVolig001-PZ1shRNA1 or saline in naive rats. The results showed mild sensory sensitization after AAVolig001-GFP injection in naive rats, comparable to the magnitudes of minor threshold changes after saline injection and to the sensitization after DRG injection of AAV in our previous reports,[33,34] but the sensory alterations were significantly much less than those after CPNI. The mild sensory changes after AAVolig001 injection to the sciatic nerve in naive rats were normalized 2–3 weeks after injection, comparable to saline injection. Rats after CPNI showed no signs of movement deficiency after recovery from anesthesia. In the CPNI experimental design, after

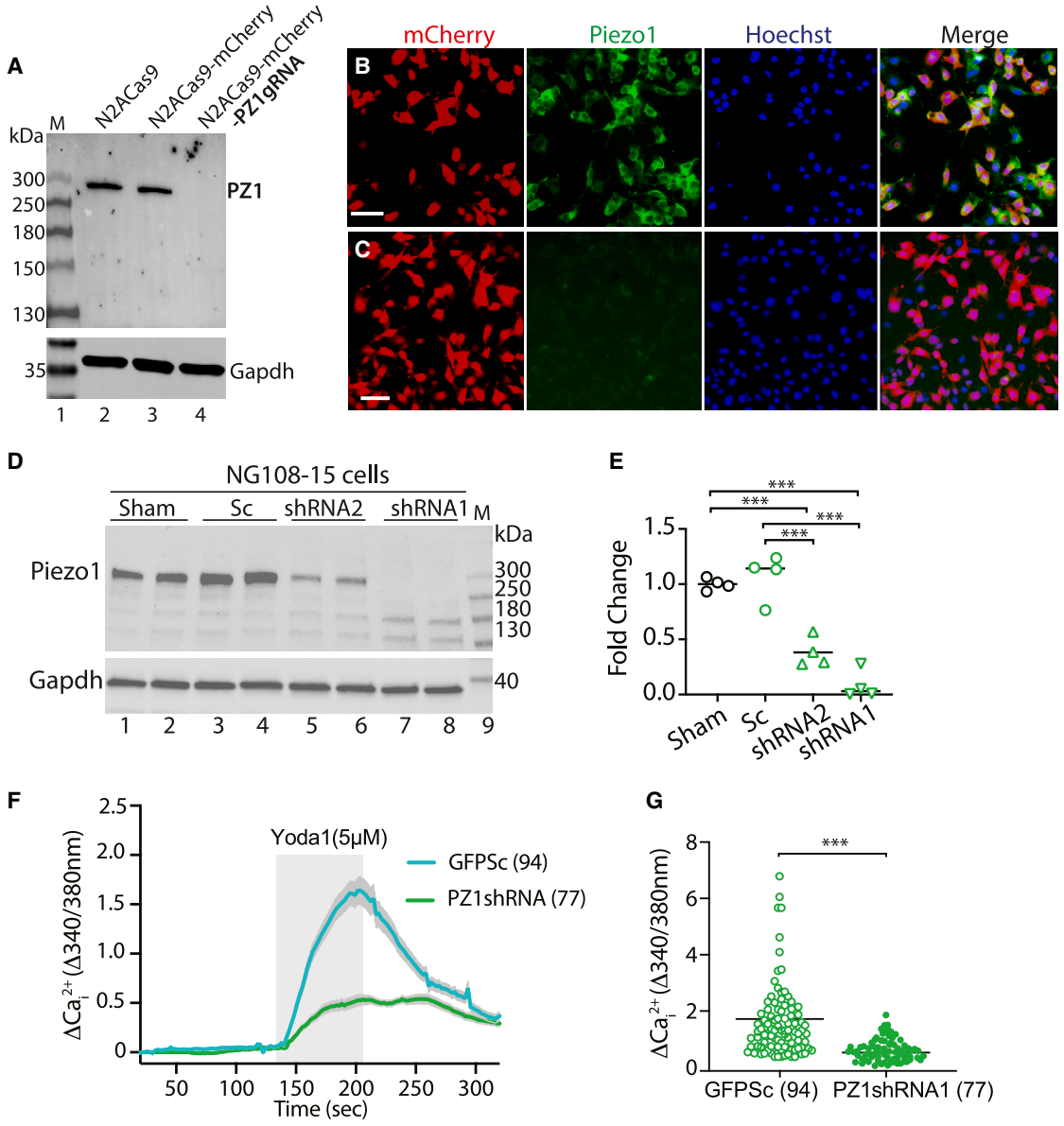

Figure 3. Cell-based Piezo1 CRISPR knockout and RNAi knockdown (NG108 cells)

(A–G) Piezo1 antibody recognizes a clean ~300-kDa band of canonical Piezo1 protein by immunoblot with comparable band density in control Cas9N2A cells and Cas9N2A cells expressing mCherry, while the Piezo1 band vanishes in the Cas9N2A cells expressing Piezo1-gRNA (A). ICC shows the detection of Piezo1 in Cas9N2A cells expressing mCherry (B), while Piezo1 signals are barely detected in the Cas9N2A cells expressing Piezo1-gRNA (C). Scale bars: 50 μm for (B) and (C). Immunoblots show Piezo1 knockdown after transfection of Piezo1shRNAs into NG108 cells (D and E). Significant reduction of Yoda1-stimulated increase of Ca_i^{2+} in NG108 cells expressing Piezo1shRNA1, compared to scramble (Sc) control (F and G).

tests of baseline (BL) sensory behaviors, rats were randomized to two groups, AAVolig001-PZ1shRNA1 and AAVolig001-Sc. Sciatic nerve injection of either vector was performed immediately after CPNI surgery, and sensory behaviors were then followed on a weekly basis for 6 weeks; after that, the animals were euthanized and tissues were harvested for IHC determination of transgene and Piezo1 expression. The results showed that all rats in both groups developed multiple modalities of pain behaviors after CPNI surgery, including the lowered threshold for withdrawal (von Frey [vF]), more frequent hyperalgesic-type responses Noxious mechanical stimulation (Pin), and hypersensitivity to heat and acetone cold stimulation. Hypersensitivity to the vF and Pin but not to thermal stimuli in CPNI rats subjected to AAVolig001-PZ1shRNA1 was moderately but significantly attenuated compared to the animals injected with the control vector

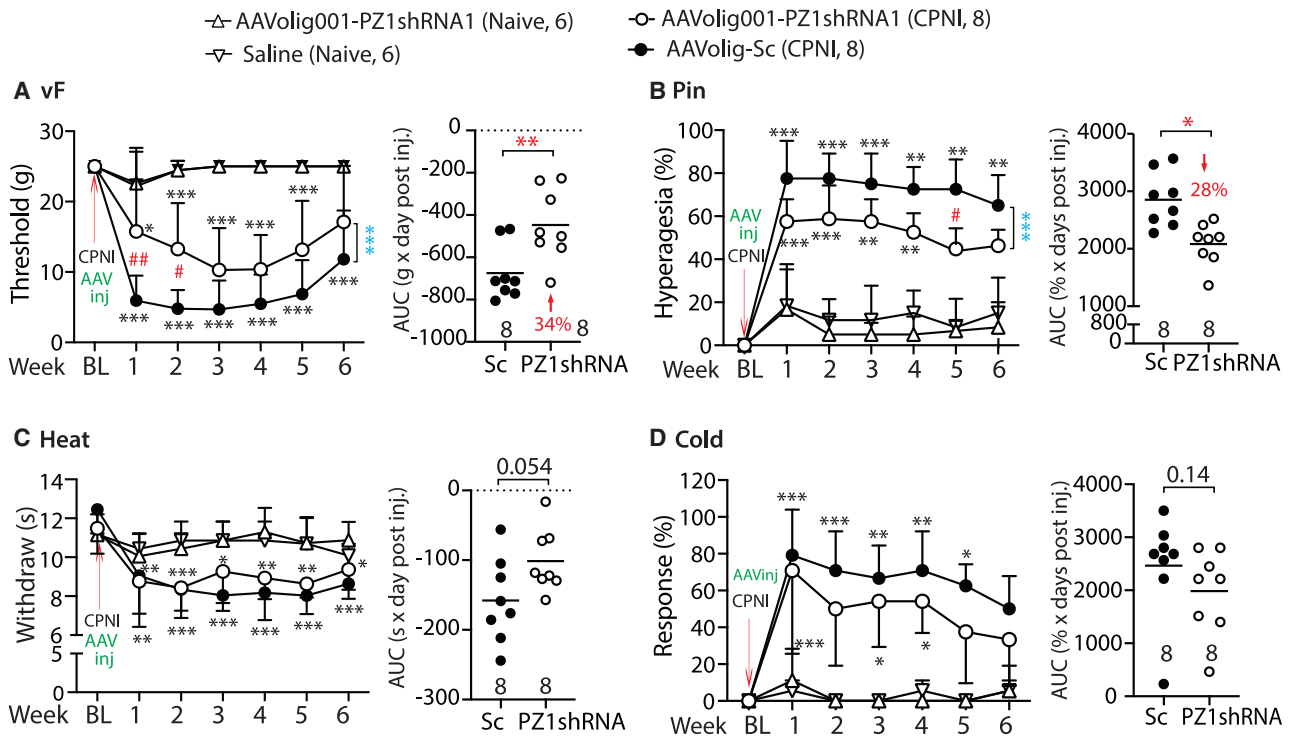

Figure 4. Mitigation of mechanical hypersensitivity in CPNI rats

(A–D) The time courses for the grouped averages to vF, Pin, heat, and cold before (BL) and after sciatic nerve injection of saline or AAVolig001-PZ1shRNA1 in naive rats and after induction CPNI immediately followed by intrasciatic injection of either AAVolig001-PZ1shRNA1 or AAVolig001-Sc. $^{*}p < 0.05$; $^{**}p < 0.01$; $^{***}p < 0.001$ for comparisons to BL within group; $^{\#}p < 0.05$; $^{\#\#}p < 0.01$ for comparisons between groups. Repeated-measures parametric two-way ANOVA for vF and heat tests and Tukey's post hoc test, and Friedman ANOVA for Pin and cold tests and Dunn's post hoc test. Blue *** is $p < 0.001$ for main effect comparison. Right sides of (A)–(D) show AUCs calculated using the measures at BL and after vector injection in CPNI rats; $^{*}p < 0.05$; $^{**}p < 0.01$; comparisons of AUCs between AAVolig001-PZ1shRNA1 and control vector, unpaired and two-tailed Student's t test.

(Figures 4A–4D). These findings suggest that the application of AAVolig001-PZ1shRNA1 early in injury-induced neuropathic pain limits the development of hypersensitivity to mechanical allodynia and hyperalgesia.

Validation of SCs-Piezo1 knockdown

IHC examination of the sciatic nerve sections revealed efficient SC transduction of AAVolig001-PZ1shRNA1 6 weeks after vector injection (Figures S3A and S3B). SC and axonal expression profile of Piezo1 immunopositivity in the rats subjected to AAVolig001-Sc was comparable to those we previously described.[14] However, the Piezo1 immunostaining signals in the SCs were apparently reduced in the rats injected with AAVolig001-PZ1shRNA1, while the axonal Piezo1 immunopositivity was comparable to the controls (Figures 5A–5D). Immunoblots of primary cultured SCs isolated from the sciatic nerve after AAV injection showed a significant reduction of Piezo1 protein in primary cultured SCs expressing PZ1shRNA1 (Figures 5E–5G). Primary cultured SCs from control animals exhibited a robust response to the Yoda1 stimulation by an increase of Ca_i^{2+}, while this Yoda1-evoked Ca_i^{2+} response was significantly reduced in the SCs expressing PZ1shRNA1 (identified by GFP signals) (Figures 5H and 5I). Piezo1 is expressed in DRG neurons and satellite glia.[10,14] However, we did not observe GFP-PZ1shRNA1 signal in DRG sections after AAVolig001-PZ1shRNA1 injection, similar to AAVolig001-Sc injection (Figure S1A). IHC revealed a comparable profile of DRG Piezo1 expression between AAVolig001-Sc and AAVolig001-PZ1shRNA1 (Figure S3C), suggesting that Piezo1 within DRG is not affected after sciatic nerve injection of AAVolig001-PZ1shRNA1. These data verify Piezo1 knockdown in the SCs after intrasciatic delivery of AAVolig001-PZ1shRNA1.

Tibial nerve delivery AAVolig001-PZ1shRNA1 improves terminal SC transduction and enhances mechanical analgesia

AAVolig001-CBA-PZ1shRNA exhibits selective SC tropism with an *in vivo* biodistribution restricted within the sciatic nerve after AAV intrasciatic delivery. To address whether tibial nerve injection may facilitate the viral particle spread and transduction of terminal sensory SCs, thereby enhancing analgesia, we injected AAVolig001-PZ1shRNA1 (same dose as sciatic delivery) into the tibial nerve using the comparable protocol (CPNI immediately followed by AAV injection). Non-noxious vF and noxious hyperalgesic Pin test, which is specifically associated with place avoidance,[35] were then evaluated for 6 weeks. Results showed that IHC staining of the tibial nerve (Figure S4) and innervating cutaneous tissue revealed efficient transduction in the terminal SCs, including $Sox10^{+}$ sensory SCs, 6 weeks after AAVolig001-PZ1shRNA1 delivery

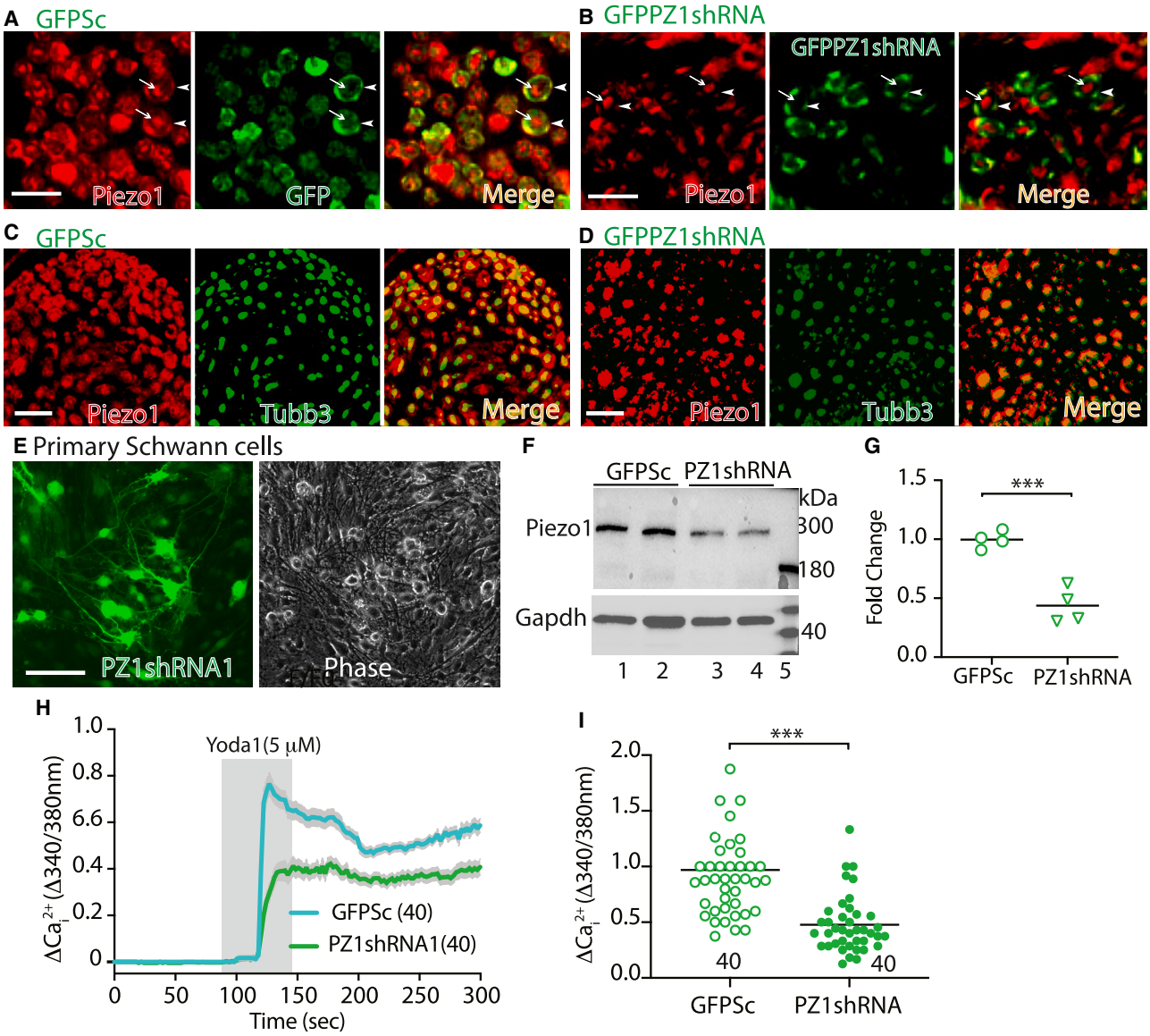

Figure 5. Validation of *in vivo* SCs-Piezo1 knockdown

(A–D) Representative IHC montage images of sciatic nerve sections illustrate PZ1 immunopositivity in control vector transduced ring-like SCs (green, arrowheads) and non-transduced axons (red, arrows) (A), while SCs-Piezo1 immunostaining signals (arrowheads) are apparently reduced in AAVolig001-PZ1shRNA1 injected rats (B). PZ1 co-stained with Tubb3 from GFP-Sc (C) and GFP-PZ1shRNA (D). (E–G) Immunoblots show that the Piezo1 protein level in GFP-PZ1shRNA1-expressing primary cultured SCs (E) is significantly reduced as compared to naive and GFP-Sc control (F and G). (H and I) Primary cultured SCs from control animals exhibit an increase in Ca_i^{2+} responding to Yoda1 stimulation, while this Yoda1-evoked response is significantly reduced in the SCs expressing PZ1shRNA1 (identified by GFP signals) (H and I). Scale bar (μm): (A-D) 10, (E) 100 and (F) 50.

via the tibial nerve. CPNI-induced mechanical allodynia and hyperalgesia were also partially reduced, but apparently with higher reversal magnitude for both allodynia and hyperalgesia than those of vector intrasciatic nerve injection (Figure 6; cf. Figure 4).

DISCUSSION

Our findings show that AAVolig001 has primary SC tropism via intraneural delivery in rats and that AAVolig001-PZ1shRNA-mediated selective RNAi silencing of Piezo1 in both mSCs and nmSCs moderately alleviates the mechanical hypersensitization representing allodynia and hyperalgesia following peripheral nerve injury. Cold and heat hypersensitivity is not significantly affected. The results support the participation of SCs-Piezo1 in the modulation of peripheral nerve mechanosensation and that Piezo1 may function as one of the mechanotransducers in the SCs that are involved in decoding injury-induced mechanical dermatome forces into afferent nociceptive hypersensitization.[36,37]

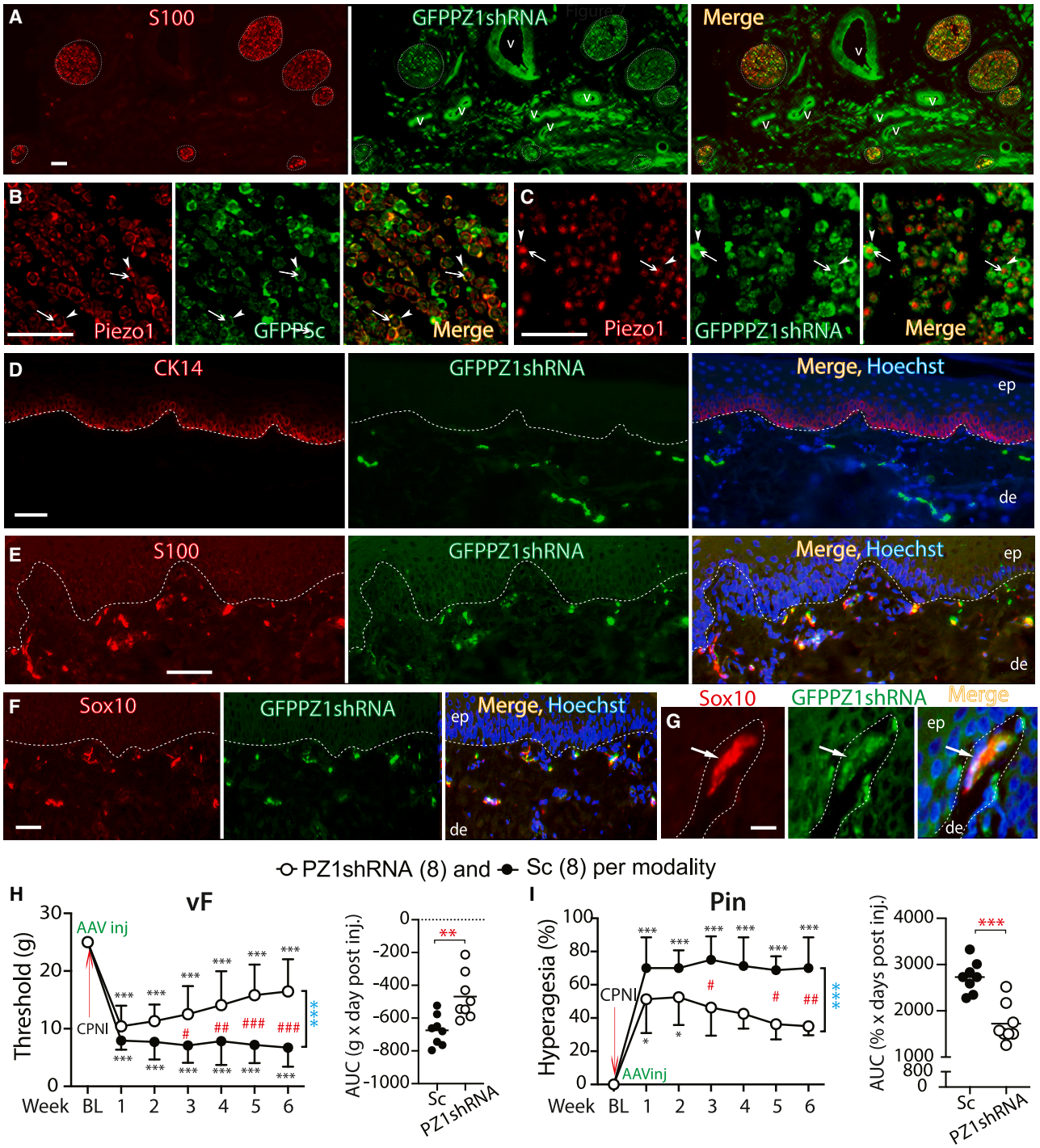

Figure 6. Tibial injection of AAVolig001-PZ1shRNA1 facilitates skin SCs transduction

(A–G) Representative IHC montage images on hindpaw glabrous skin sections after tibial nerve GFP-PZ1shRNA injection. GFP staining (green), colabeled with S100 (red) on the nerve bundles (dashed circles), v denotes vessels (A). GFP staining colabeled with PZ1 in subcutaneous nerve bundles from control vector GFP-Sc (B) and GFP-PZ1shRNA (C); arrowheads and arrows point to axonal PZ1 and SCs-PZ1, respectively. GFP staining colabeled with CK14 (D), S100 (E), and Sox10 (F). (G) Meissner corpuscle colabeled with GFP with Sox10. Scale bars (μm): (A)–(F) 50 and (G) 10. (H and I) The time courses for the grouped averages to vF (H) and Pin (I) at BL and after tibial nerve AAV injection in CPNI rats ($n = 8$ per group). $^{*}p < 0.05$; $^{***}p < 0.001$; one-way ANOVA and Tukey post hoc, compared to BL; $^{\#}p < 0.05$; $^{\#\#}p < 0.01$; $^{\#\#\#}p < 0.001$, compared between groups; blue *** denotes the comparisons of grouped main effects. Right sides of (H) and (I) are AUCs; $^{**}p < 0.01$; $^{***}p < 0.001$; unpaired and two-tailed Student t tests.

As noted, although AAVolig001-PZ1shRNA induces selective SC expression and silencing of Piezo1 in both mSCs and nmSCs via sciatic nerve delivery, the mechanical hypersensitization following CPNI is only partially reversed. This could be due to several possible reasons. First, Piezo1 is also expressed in the afferent axons that are spared transduction by AAVolig00-CBA-PZ1shRNA, and thus, the total biological effects on antinociception are compromised. Second, Piezo1 in cutaneous sensory SCs is more important since sensory SCs are a subset of specialized cutaneous SCs located in the epidermal-dermal border, directly sensing mechanical nociception and playing a crucial role in initiating and transmitting mechanical nociceptive signals.[6,38] PZ1shRNA transduction in cutaneous SCs via tibial nerve delivery of AAVolig001-PZ1shRNA shows enhancement of mitigation of mechanical hypersensitization of CPNI, compared to vector intrasciatic delivery. This provides evidence supporting the importance of sensory SCs in mechanosensory function. Furthermore, both Piezo1 and Piezo2 are coexpressed in the SCs, including cutaneous sensory SCs,[14,39] and Piezo2 has a proven role in nociception Partial reversal of mechanical hypersensitization by silencing of only Piezo1 may suggest that Piezo1 and Piezo2 in the SCs have some functional redundancy in mechanosensation and that Piezo2 may provide functional complementary effects when Piezo1 is ablated. Future studies need to investigate the effects of AAVolig001-mediated selective silencing of SCs-Piezo2 and a combined knockdown of both SCs-Piezo1/2 on peripheral nerve mechanosensation and pain pathogenesis.

SCs are inherently mechanosensitive, which is important for PNS development, myelination, and regulation of sensory neurons[40,41]; thus, gene transfer to manipulate SCs may have diverse therapeutic potential.[42] However, a significant issue for *in vivo* investigation of the roles of SCs, such as Piezo channels, in peripheral nociception is the lack of pharmacological and genetic tools that selectively target both mSCs that transmit touch and nmSCs that accommodate nociceptive nerve fibers.[43] AAV vectors are very useful tools for selective manipulation of the gene and the associated molecular pathways for studying mechanisms and for the therapy of various PNS disorders. However, no AAV capsid has been described in the literature as exhibiting primary tropism to both mSCs and nmSCs when a constitutive promoter drives transcription. Intrasciatic AAV9 with a constitutive potent promoter (CAG) has been shown to have efficient transduction to mSCs,[44] but another study reports that intrasciatic AAV9 incorporating the CMV promoter induces more widespread effects, with both SCs and other cell types transduced, including motor and sensory neurons.[45] AAV incorporating an MPZ promoter for transcription and packed by serotype 9 has shown efficient *in vivo* transduction to SCs.[46] However, since MPZ is known to be expressed exclusively in the mSCs,[47] this approach, although powerful for the investigation of mSCs, is not sufficient to study the role of nmSCs in peripheral nociception. AAV serotype 8 with a CMV promoter via direct sciatic nerve injection also transduces SCs[48]; however, other studies show that sciatic nerve injection of AAV8 efficiently transduces sensory neurons.[49] Our data reveal that, comparable to the other reports,[50,51] sciatic nerve injection of AAV6 with CBA promoter for transcription induces widespread non-cell-specific transgene expression in SCs, afferent axons, sensory neuron somata, and central and peripheral terminals, as well as motor neurons in the ventral horn via retrograde transduction (Figure 2). Lentiviral vector and nanoparticles have been tested for *in vivo* mSC transduction,[52,53] but AAVs have superiority and are a predominant tool for *in vivo* transduction. Most current AAV capsid serotypes (using CBA or CMV promoter for transcription) via different delivery routes transduce neurons at a much higher rate than any other neural cell types, making it challenging to manipulate SCs selectively.[54] Thus, true SC-specific targeting for both mSCs and nmSCs remains elusive. AAV serotype olig001, which is a capsid with a chimeric serotype composed of AAV1, -2, -6, -8, and -9, has exclusive oligodendrocyte tropism after delivery to the brain, and *in vitro* tests confirm that AAVOlig001 has a greater binding affinity for oligodendrocyte surface receptors than AAV8.[15] We verify in this report that AAVolig001 also determines selective transduction to SCs via intraneural delivery without the need for incorporating SC-specific transcription elements in the vector construct. AAVolig001 has unique and selective primary tropism to both mSCs and nmSCs following the intraneural delivery, which limits potential undesirable effects in other cells and sites along the PNS that may present as confounding factors in data interpretation.

Occurrence of sciatic nerve injection injury (SNII) after sciatic nerve injection may induce severe sensory disturbance and motor loss with poor recovery when delivery of toxic chemicals and the needle tips are inserted into intrafascicular, while extrafascicular space injection normally produces no or minimal nerve injury.[55,56] About 50% of the cross-sectional area in the 4-month-old rats is non-neural tissue, and 50% of the total cross-section inside the sciatic nerve epineurium in humans consists of non-neural connective tissue.[57] Thus, the results of behavior evaluation indicate that our injection techniques are successful in attempts to apply injecta into the extrafascicular space, avoiding intrafascicular injection and that AAV itself is not toxic.[45,58] Although it is not possible to ascertain the needle insertion sites, the minimally traumatic delivery implies that, with the correct technique, an intrafascicular injection is a preventable event in the experimental rats by our microinjection technique, which is comparable to viral vector intrasciatic injection in mice showing injection itself causing little Wallerian degeneration and long-term behavioral adverse effects on sciatic nerve functions.[59] In comparison with genomic modification strategies such as the Cre-Loxp system, AAVolig001-based RNAi silencing facilitates fast, reproducible, and straightforward genetic manipulation of both mSCs and nmSCs *in vivo* to investigate specific molecular mechanisms in nociception, thus preventing the adaptation and compensation that frequently occur in mice with genomic modifications.[59]

MATERIALS AND METHODS

Animals

Adult male Sprague-Dawley rats with 100–125 g body weight (Charles River Laboratories, Wilmington, MA) were used. Animals were housed individually in a room maintained at constant temperature

(22°C ± 0.5°C) and relative humidity (60% ± 15%) with an alternating 12-h light-dark cycle. Animals had access to water and food *ad libitum* throughout the experiment, and all efforts were made to minimize suffering. All survival surgeries were completed in a sterile environment under a surgical microscope in animals anesthetized with isoflurane (2%–5%). For tissue harvest euthanasia, animals were deeply anesthetized by isoflurane, followed by decapitation with a well-maintained guillotine. The estimated numbers of animals needed were derived from our previous experience with similar experiments,[14,39] and a power analysis was not performed. The numbers of rats used were detailed in the relevant sections or figure legends of the experiments. Animals were randomized for each testing group.

Molecular cloning and AAV constructs (Figure 3)

AAV vectors encoding a dual promoter and bidirectional transgene cassette, in which a U6 promoter drives PZ1shRNA or an Sc RNA as control and GFP (for *in vivo* tracing) transcribed by a hybrid CMV enhancer/CBA promoter, was constructed. Two shRNAs against rat Piezo1 (NM_001077200.2) were designed using Invivogen siRNA Wizard Software (https://www.invivogen.com). PZ1shRNA1: 5′-GCC GGCCATCTTGTTTGTTTATCAAGAGTAAACAAACAAGATG GCCGGC-3′ and Piezo2: 5′-GCTGGAGGAGGATGACATAGA TCAAGAGTCTATGTCATCCTCCTCCAGC-3′ (loop sequence underlined). The DNA sequences of U6-PZ1shRNAs were synthesized and subcloned into the Mlu I site by GenScript (Piscataway, NJ) that resides upstream of the CBA promoter of the single-strand AAV-expressing plasmid (p)AAV-CBA-GFP (Figure S1), as we described previously.[60] This generated pAAV-CBA-GFP-U6-PZ1shRNAs (pAAV-PZ1shRNAs). The plasmid of pAAV-CBA-GFP-U6-Sc (pAAV-Sc), designed as we previously described,[61] was used as the control. The above plasmids were subsequently used to produce AAVs packed by capsid AAVolig001 by PackGene (Worcester, MA). An AAVolig001-CBA-GFP was provided by Myrtelle (https://myrtellegtx.com), and AAV6-CBA-GFP was produced and purified in our laboratory using our established methods.[62] Total four AAVs were used in the experiments, including (1) AAVolig001-CBA-GFP (AAVolig001-GFP, 1×10^{13} GC/mL), (2) AAVolig001-PZ1shRNA-GFP (AAVolig001-PZ1shRNA, 1.2×10^{13} GC/mL), (3) AAV olig001-Sc-GFP (AAVolig001- Sc, 2×10^{13} GC/mL), and (4) AAV6-CBA-GFP (AAV6-GFP, 2×10^{13} GC/mL).

Primary cell culture and cell lines (Figures 3 and 5)

Primary SCs cultures were performed as previously described.[14] In brief, SCs were purified by digesting with 0.25% trypsin (Sigma-Aldrich, St. Louis, MO) for a short time (10–20 s) to obtain > 80% pure SCs, as determined by ICC with S100, an SC marker. NG108-15 (NG108) cells were obtained from American Type Culture Collection (Manassas, VA). N2A cells stably expressing CRISPR-Cas9 nuclease (Cas9N2A) were obtained from GeneCopoeia (Rockville, MD). These cells were cultured by a standard protocol using Dulbecco's modified Eagle's medium supplemented with 10% fetal bovine serum and antibiotics (Thermo Fisher, Waltham, MA) and were grown at 37°C and in 5% CO_2 in a humidified incubator.

Microfluorimetric Ca^{2+} imaging (Figures 3 and 5)

Determination of Ca_i^{2+} was performed using Fura2-based microfluorimetry and imaging analysis, as we previously described.[63] Cells were imaged to monitor Ca_i^{2+} responses to Yoda1 perfusion (1 min), and total DMSO concentration was kept $\leq$1% for all tested Yoda1 concentrations. The Ca_i^{2+} was evaluated as the ratio of emission in response to excitation at 340 and 380 nm, expressed as the 340/380 nm fluorescence emission ratio ($R_{340/380}$) that is directly correlated to the amount of Ca_i^{2+}.[64] A $\geq$30% increase in $R_{340/380}$ from BL after superfusion with Yoda1, expressed as ΔCa^{2+} (Δ340/380nm), was considered a positive response for all cells recorded.[14,65]

AAV sciatic and tibial nerve injection (Figures 4 and 6)

AAV was injected into either sciatic nerve or tibial nerve using a procedure similar to what we described for DRG injection via a microprocessor-controlled injector (Nanoliter 2000, World Precision Instruments, Sarasota, FL)[34] and comparable to a protocol described for sciatic nerve injection in mice.[44,59,66] Briefly, after appropriate anesthesia was obtained by the inhalation of 2% isoflurane, we exposed the right sciatic nerve or tibial nerve through a lateral incision of the middle thighs and division of the superficial fascia and muscle under aseptic conditions, and the sciatic nerve and tibial nerve were exposed at a point proximal to the bifurcation. Rats received sciatic or tibial nerve injection at 3–5 mm distal to the bifurcation of AAVolig001-GFP injection in a dose of 2×10^{11} GC (20 μL) containing 0.1% Fast Green (0.1 μL) in the viral vector solution to visualize the injected solution. AAV was injected directly into subepineural space (beneath the clear fascia surrounding the nerve but outside the perineurium) with a pulled glass capillary tip (40–60 μm diameter) inserted into the nerves (~10 mm), forming an angle with the longitudinal axis of the nerves over a 5-min period using a microprocessor-controlled injection system employing direct piston displacement mounted on a micromanipulator. Once penetration was achieved, the injector was backed off until the compression of the tissue was not evident to lessen tissue pressure on the pipette aperture. Removal of the glass pipette was delayed for an additional 5 min at a rate of 0.5 μL/min to minimize the extrusion of the injectate. Following the injection and closure of overlying muscle and skin, the animals were returned to their housing, where they remained as the designed experiments required. Saline (20 μL) was injected as the control for the comparative evaluation of the sensory behavior of injection and AAV.

Animal pain model and behavior testing (Figures 4 and 6)

For CPNI, animals were anesthetized using isoflurane at 4% for induction and 2% for maintenance. Under anesthesia, the right sciatic nerve was exposed under aseptic surgical conditions by blunt dissection of the femoral biceps muscle. The sciatic nerve and its three branches (sural, common peroneal, and tibial nerves) were isolated. CPNI surgery was performed using a modification of a method previously validated in rats.[67] Specifically, after exposure of the sciatic nerve and its three branches, the CPN was then tightly ligated and transected distal to the ligation (leaving the tibial and sural nerve intact). The overlying muscle and skin were then sutured following

surgery. Sham-operated rats were subjected to all preceding procedures without nerve ligation or transection.

Sensory behavioral evaluation (Figures 4 and 6)

Behavioral tests were conducted between 9:00 a.m. and 12:00 p.m. Animals were habituated in individual test compartments for at least 1 h before each test. Behavior tests were carried out as previously described[34] and were performed by personnel blinded to treatments. Stimuli were applied to the hindpaw plantar skin in the tibial nerve innervating area for CPNI and in the sural nerve innervating area for TNI.

(1) Mild mechanical stimulation (vF). The withdrawal threshold was determined using calibrated monofilaments (Patterson Medical, Bolingbrook, IL) with forces of 0.3, 0.5, 0.8, 1.0, 2.8, 5, 9, 14, and 24 g, applied in an up-down fashion, allowing calculation of the 50% withdrawal threshold.[68] Beginning with the 2.8-g filament, filaments were applied to the plantar skin with just enough force to bend the fiber and held for 1 s. If a response was observed, then the next smaller filament was applied, and if no response was observed, the next larger was applied until a reversal occurred, defined as a withdrawal after a previous lack of withdrawal, or vice versa. Following a reversal event, four more stimulations were performed following the same pattern. The forces of the filaments before and after the reversal and the four filaments applied following the reversal were used to calculate the vF threshold. Rats not responding to any filament were assigned a score of 25g.
(2) Noxious mechanical stimulation (Pin). The point of a 22-g spinal anesthesia needle was gently applied five times to the plantar surface of the hindpaw with enough force to indent but not puncture the skin. Five applications were separated by at least 10 s, which was repeated after 2 min, for a total of 10 touches. For each application, this evokes either a simple withdrawal response with immediate return of the foot to the cage floor or a response characterized by sustained elevation with grooming (e.g., licking or chewing the toes) and possibly shaking, lasting at least 1 s. The latter behavior is referred to as hyperalgesia behavior. This hyperalgesia response has been associated specifically with an aversive experience.[35]
(3) Heat stimulation. This was performed using a device designed to identify heat sensitivity (Paw Thermal Stimulator System, University Anesthesia Research & Development Group, San Diego, CA). Rats were placed on a temperature-regulated glass platform heated to 30°C, and the lateral plantar surface of the hindpaw was stimulated with a radiant heat source (50 W halogen bulb) directed through an aperture. The time elapsed from the initiation of the stimulus until withdrawal (withdrawal latency) as detected by a series of photocells was measured. Each hindpaw was tested four times, and the withdrawal latency values were averaged.
(4) Cold stimulation. Acetone was applied from a syringe attached to PE220 tubing to make a meniscus that was touched to the plantar surface of the hindpaw, such that the drop spread out on the plantar surface of the paw without contact of the tubing to the skin. Each hindpaw was tested three times in an alternating fashion. Any withdrawal was considered a positive response. The frequency of withdrawal from the stimulus was recorded.

Validation of Piezo1 antibody in CRISPR-Cas9-mediated Piezo1 knockout cells (Figure 3)

Lentiviral expression plasmid pWPT-mCherry was used to express dual CRISPR gRNAs specific to human Piezo1 (gRNA1: 5′-AGCAT TGAAGCGTAACAGGG-3′, gRNA2: 5′-AGAGAGCATTGAA GCGTAAC-3′), as described previously.[14] Lentivectors expressing mCherry (control) or dual Piezo1 gRNAs were packaged using pWPT-mCherry and pWPT-mCherry-PZ1gRNAs with packaging plasmid pCMVDR8.74 and envelope plasmid pVSV-g and products titrated in the range of 1×10^6–1×10^7 transduction unit/mL, as previously reported.[14] Cultured Cas9N2A cells grown to 50% confluence were infected by LV-mCherry-PZ1gRNAs or LV-mCherry-Sc (control) in the presence of 8 μg/mL polybrene (Sigma-Aldrich) at an optimized multiplicity of infection 5.

Tissue harvest for IHC and immunoblots

The rats were ∼4 months old when tissues were harvested. After transcardial perfusion with cold 100 mL PBS, lumbar (L) 4 and 5 DRG, lumbar spinal cord, and sciatic nerve segments proximal to the sciatic bifurcation and terminal branches, as well as hindpaw glabrous skin, were dissected and fixed in Richard-Allan Scientific Buffered Zinc Formalin (Thermo Fisher) overnight, followed by processing for paraffin embedment. The previously described histological protocol was adopted.[39]

ICC and IHC (Figures 1, 2, 3, 6, and S1–S4)

ICC on cultured cells and IHC on tissue sections were performed according to standard procedures.[69] Non-specific binding was reduced by incubating the sections for 30 min with a solution of 5% BSA in PBS plus 0.05% Tween 20. Cells and tissue sections were immunolabeled with the selected primary antibodies mouse Piezo1 (1:400, Novus Biologicals, NBP2-75617), rabbit GFP (1:500, Cell Signaling Technology [Danvers, MA], 2555S), rabbit mCherry (1:400, Cell Signaling Technology, 43590), rabbit GAP43 (1:400, Cell Signaling Technology, 8945), rabbit p75NTR (1:400, Cell Signaling Technology, 8238), rabbit MPZ (1:1,000, Cell Signaling Technology, 57518s), rabbit S100 (1:1,000, Cell Signaling Technology, 13018), goat MBP (1:1,000, Santa Cruz Biotechnology [SCB], sc13912), goat Sox10 (1:200, SCB, sc17342), rabbit NF200 (1:1,000, Cell Signaling Technology, 30564), rabbit Tubb3 (1:1,000, Cell Signaling Technology, 5586), mouse cytokeratin14 (CK14, 1:200, SCB, sc53253), and rabbit glial fibrillary acidic protein (1:1,000, Dako [Glostrup, Denmark, Z0334) in a humid atmosphere overnight at 4°C. The fluorophore-conjugated (Alexa 488 or Alexa 594, 1:2,000) secondary antibodies (Jackson ImmunoResearch, West Grove, PA) were used to reveal immune complexes. The immunostaining was examined, and images were captured using a Nikon TE2000-S fluorescence microscope (El Segundo, CA), with filters suitable for selectively detecting the green and red fluorescence using a QuantiFire digital camera (Optronics,

Ontario, NY). NIH ImageJ software (http://rsbweb.nih.gov/ij/) was used for analysis. For double-label colocalization, images from the same specimen but showing different antigen signals were overlaid by digitally merging the captured images, which were brightness/contrast-adjusted for optical quality. Positive immunostaining was defined as fluorescence intensity greater than average background fluorescence plus 2 standard deviations (SDs) of the cells in an adjacent section in the same slide of negative control (the first antibody omitted) under identical acquisition parameters ($n = 10$ for different markers). The AAVoligo001-GFP transduction rate in SCs was estimated on the GFP/markers (MPZ or P75NTR) double-stained images. When counting, image contrast was adjusted such that background levels became inapparent, and the same cutoff level was used for all images. The numbers of GFP^+ green rings and red-labeled markers (MPZ or P75NTR) were counted in green and red images, respectively, and the percentage of GFP^+ SCs out of marker-positive SCs in the merged images was calculated.

Immunoblots (Figures 3 and 5)

Immunoblots of cell lysates were performed as described previously.[39] Immunoreactive proteins were detected by Pierce enhanced chemiluminescence (Thermo Fisher) on a ChemiDoc Imaging system (Bio-Rad, Hercules, CA) after incubation with horseradish peroxidase-conjugated second antibodies (1:5,000, Bio-Rad). The densitometry of the selected bands was analyzed by NIH ImageJ software.

Statistical analysis

The statistical analysis was performed with GraphPad Prism 9 (GraphPad Software, San Diego, CA). The numbers of biological replicates (e.g., animals, cells, immunoblot samples) are provided in the corresponding figures and legends. No data points were excluded. Mechanical allodynia (vF), hyperalgesia (Pin), and thermal (heat and cold) changes after sciatic nerve injection were compared to pre-injection BL with repeated measures of two-way ANOVA and Tukey post hoc for vF and heat, and Friedman's tests and Dunn's post hoc for Pin and cold. The area under the curves (AUC) was compared among groups by one-way ANOVA and Student's t test, where appropriate. The results are reported as means and SDs. Differences were significant for values at $p < 0.05$.

DATA AVAILABILITY

Data for the materials, including plasmid nucleotide sequences (text) of pAAV-CBA-PZ1shRNA and pWPT-PZ1-CRISPRgRNA with annotations of key components of the constructs, behavior test value data, calcium imaging value data, and full unedited western blot images will be deposited as of the date of publication for the research community through the public repository Dataverse.

ACKNOWLEDGMENTS

This research was supported by National Institutes of Health grants 1R21NS138704-01 (H.Y.), R33NS116203 (H.Y.), R01 NS070711 (C.L.S.), R37 NS108278 (C.L.S.), the Javits award, the 2022 and 2023 awards from the Dr. Ralph and Marian Falk Medical Research Trust, Bank of America, private bank (H.Y.), and support from Myrtelle.

AUTHOR CONTRIBUTIONS

H.Y. conceived and designed the study. S.M.S. and H.Y. wrote the manuscript. Q.H.H. and C.L.S. helped review and revise the manuscript. S.M.S., B.I.-Z., U.G., A.M., C.Q., F.F., and H.Y. performed the experiments, analyzed the data, and organized all the figures. H.Y. and C.L.S. obtained the funding.

DECLARATION OF INTERESTS

The authors declare no competing interests.

SUPPLEMENTAL INFORMATION

Supplemental information can be found online at https://doi.org/10.1016/j.omtm.2025.101433.

REFERENCES

1. Campana, W.M. (2007). Schwann cells: activated peripheral glia and their role in neuropathic pain. Brain Behav. Immun. *21*, 522–527.
2. Wei, Z., Fei, Y., Su, W., and Chen, G. (2019). Emerging Role of Schwann Cells in Neuropathic Pain: Receptors, Glial Mediators and Myelination. Front. Cell. Neurosci. *13*, 116.
3. Gillespie, C.S., Sherman, D.L., Fleetwood-Walker, S.M., Cottrell, D.F., Tait, S., Garry, E.M., Wallace, V.C., Ure, J., Griffiths, I.R., Smith, A., and Brophy, P.J. (2000). Peripheral demyelination and neuropathic pain behavior in periaxin-deficient mice. Neuron *26*, 523–531.
4. Ding, Y.Q., and Qi, J.G. (2022). Sensory root demyelination: Transforming touch into pain. Glia *70*, 397–413.
5. De Logu, F., Nassini, R., Materazzi, S., Carvalho Gonçalves, M., Nosi, D., Rossi Degl'Innocenti, D., Marone, I.M., Ferreira, J., Li Puma, S., Benemei, S., et al. (2017). Schwann cell TRPA1 mediates neuroinflammation that sustains macrophage-dependent neuropathic pain in mice. Nat. Commun. *8*, 1887.
6. Abdo, H., Calvo-Enrique, L., Lopez, J.M., Song, J., Zhang, M.D., Usoskin, D., El Manira, A., Adameyko, I., Hjerling-Leffler, J., and Ernfors, P. (2019). Specialized cutaneous Schwann cells initiate pain sensation. Science *365*, 695–699.
7. Coste, B., Mathur, J., Schmidt, M., Earley, T.J., Ranade, S., Petrus, M.J., Dubin, A.E., and Patapoutian, A. (2010). Piezo1 and Piezo2 are essential components of distinct mechanically activated cation channels. Science *330*, 55–60.
8. Ranade, S.S., Syeda, R., and Patapoutian, A. (2015). Mechanically Activated Ion Channels. Neuron *87*, 1162–1179.
9. Szczot, M., Liljencrantz, J., Ghitani, N., Barik, A., Lam, R., Thompson, J.H., Bharucha-Goebel, D., Saade, D., Necaise, A., Donkervoort, S., et al. (2018). PIEZO2 mediates injury-induced tactile pain in mice and humans. Sci. Transl. Med. *10*, eaat9892.
10. Hill, R.Z., Loud, M.C., Dubin, A.E., Peet, B., and Patapoutian, A. (2022). PIEZO1 transduces mechanical itch in mice. Nature *607*, 104–110.
11. Lai, A., Cox, C.D., Chandra Sekar, N., Thurgood, P., Jaworowski, A., Peter, K., and Baratchi, S. (2022). Mechanosensing by Piezo1 and its implications for physiology and various pathologies. Biol. Rev. Camb. Phil. Soc. *97*, 604–614.
12. Acheta, J., Bhatia, U., Haley, J., Hong, J., Rich, K., Close, R., Bechler, M.E., Belin, S., and Poitelon, Y. (2022). Piezo channels contribute to the regulation of myelination in Schwann cells. Glia *70*, 2276–2289.
13. Manganas, P., Kavatzikidou, P., Kordas, A., Babaliari, E., Stratakis, E., and Ranella, A. (2022). The role of mechanobiology on the Schwann cell response: A tissue engineering perspective. Front. Cell. Neurosci. *16*, 948454.
14. Shin, S.M., Itson-Zoske, B., Fan, F., Gani, U., Rahman, M., Hogan, Q.H., and Yu, H. (2023). Peripheral sensory neurons and non-neuronal cells express functional Piezo1 channels. Mol. Pain *19*, 17448069231174315.
15. Powell, S.K., Khan, N., Parker, C.L., Samulski, R.J., Matsushima, G., Gray, S.J., and McCown, T.J. (2016). Characterization of a novel adeno-associated viral vector with preferential oligodendrocyte tropism. Gene Ther. *23*, 807–814.
16. Francis, J.S., Markov, V., Wojtas, I.D., Gray, S., McCown, T., Samulski, R.J., Figueroa, M., and Leone, P. (2021). Preclinical biodistribution, tropism, and efficacy of oligotropic AAV/Olig001 in a mouse model of congenital white matter disease. Mol. Ther. Methods Clin. Dev. *20*, 520–534.
17. Ling, Q., Herstine, J.A., Bradbury, A., and Gray, S.J. (2023). AAV-based *in vivo* gene therapy for neurological disorders. Nat. Rev. Drug Discov. *22*, 789–806.

18. Bosch-Queralt, M., Fledrich, R., and Stassart, R.M. (2023). Schwann cell functions in peripheral nerve development and repair. Neurobiol. Dis. *176*, 105952.

19. Muzio, M.R., Fakoya, A.O., and Cascella, M. (2025). Histology, Axon. [Updated 2022 Nov 14]. In StatPearls (Treasure Island (FL): StatPearls Publishing), https://www.ncbi.nlm.nih.gov/books/NBK554388/.

20. Jessen, K.R., and Mirsky, R. (2005). The origin and development of glial cells in peripheral nerves. Nat. Rev. Neurosci. *6*, 671–682.

21. Follis, R.M., Tep, C., Genaro-Mattos, T.C., Kim, M.L., Ryu, J.C., Morrison, V.E., Chan, J.R., Porter, N., Carter, B.D., and Yoon, S.O. (2021). Metabolic Control of Sensory Neuron Survival by the p75 Neurotrophin Receptor in Schwann Cells. J. Neurosci. *41*, 8710–8724.

22. Curtis, R., Stewart, H.J., Hall, S.M., Wilkin, G.P., Mirsky, R., and Jessen, K.R. (1992). GAP-43 is expressed by nonmyelin-forming Schwann cells of the peripheral nervous system. J. Cell Biol. *116*, 1455–1464.

23. Griffin, J.W., and Thompson, W.J. (2008). Biology and pathology of nonmyelinating Schwann cells. Glia *56*, 1518–1531.

24. Ma, B., Yin, C., Hu, D., Newman, M., Nicholls, P.K., Wu, Z., Greene, W.K., and Shi, Z. (2018). Distribution of non-myelinating Schwann cells and their associations with leukocytes in mouse spleen revealed by immunofluorescence staining. Eur. J. Histochem. *62*, 2890.

25. Yao, M., Tijore, A., Cheng, D., Li, J.V., Hariharan, A., Martinac, B., Tran Van Nhieu, G., Cox, C.D., and Sheetz, M. (2022). Force- and cell state-dependent recruitment of Piezo1 drives focal adhesion dynamics and calcium entry. Sci. Adv. *8*, eabo1461.

26. Li, J.V., Ng, C.A., Cheng, D., Zhou, Z., Yao, M., Guo, Y., Yu, Z.Y., Ramaswamy, Y., Ju, L.A., Kuchel, P.W., et al. (2021). Modified N-linked glycosylation status predicts trafficking defective human Piezo1 channel mutations. Commun. Biol. *4*, 1038.

27. Vadakkan, K.I., Jia, Y.H., and Zhuo, M. (2005). A behavioral model of neuropathic pain induced by ligation of the common peroneal nerve in mice. J. Pain *6*, 747–756.

28. Hellman, A., Maietta, T., Clum, A., Byraju, K., Raviv, N., Staudt, M.D., Jeannotte, E., Nalwalk, J., Belin, S., Poitelon, Y., and Pilitsis, J.G. (2021). Development of a common peroneal nerve injury model in domestic swine for the study of translational neuropathic pain treatments. J. Neurosurg. *135*, 1516–1523.

29. Wiesenfeld-Hallin, Z. (1988). Partially overlapping territories of nerves to hindlimb foot skin demonstrated by plasma extravasation to antidromic C-fiber stimulation in the rat. Neurosci. Lett. *84*, 261–265.

30. Gangadharan, V., Zheng, H., Taberner, F.J., Landry, J., Nees, T.A., Pistolic, J., Agarwal, N., Männich, D., Benes, V., Helmstaedter, M., et al. (2022). Neuropathic pain caused by miswiring and abnormal end organ targeting. Nature *606*, 137–145.

31. Duraku, L.S., Hossaini, M., Hoendervangers, S., Falke, L.L., Kambiz, S., Mudera, V.C., Holstege, J.C., Walbeehm, E.T., and Ruigrok, T.J.H. (2012). Spatiotemporal dynamics of re-innervation and hyperinnervation patterns by uninjured CGRP fibers in the rat foot sole epidermis after nerve injury. Mol. Pain *8*, 61.

32. Jeon, S.M., Pradeep, A., Chang, D., McDonough, L., Chen, Y., Latremoliere, A., Crawford, L.K., and Caterina, M.J. (2024). Skin Reinnervation by Collateral Sprouting Following Spared Nerve Injury in Mice. J. Neurosci. *44*, e1494232024.

33. Fischer, G., Pan, B., Vilceanu, D., Hogan, Q.H., and Yu, H. (2014). Sustained relief of neuropathic pain by AAV-targeted expression of CBD3 peptide in rat dorsal root ganglion. Gene Ther. *21*, 44–51.

34. Fischer, G., Kostic, S., Nakai, H., Park, F., Sapunar, D., Yu, H., and Hogan, Q. (2011). Direct injection into the dorsal root ganglion: technical, behavioral, and histological observations. J. Neurosci. Methods *199*, 43–55.

35. Wu, H.E., Gemes, G., Zoga, V., Kawano, T., and Hogan, Q.H. (2010). Learned avoidance from noxious mechanical simulation but not threshold semmes weinstein filament stimulation after nerve injury in rats. J. Pain *11*, 280–286.

36. Corfas, G., Velardez, M.O., Ko, C.P., Ratner, N., and Peles, E. (2004). Mechanisms and roles of axon-Schwann cell interactions. J. Neurosci. *24*, 9250–9260.

37. Samara, C., Poirot, O., Domènech-Estévez, E., and Chrast, R. (2013). Neuronal activity in the hub of extrasynaptic Schwann cell-axon interactions. Front. Cell. Neurosci. *7*, 228.

38. Ojeda-Alonso, J., Calvo-Enrique, L., Paricio-Montesinos, R., Kumar, R., Zhang, M.D., Poulet, J.F.A., Ernfors, P., and Lewin, G.R. (2024). Sensory Schwann cells set perceptual thresholds for touch and selectively regulate mechanical nociception. Nat. Commun. *15*, 898.

39. Shin, S.M., Moehring, F., Itson-Zoske, B., Fan, F., Stucky, C.L., Hogan, Q.H., and Yu, H. (2021). Piezo2 mechanosensitive ion channel is located to sensory neurons and nonneuronal cells in rat peripheral sensory pathway: implications in pain. Pain *162*, 2750–2768.

40. Rouach, N., Avignone, E., Même, W., Koulakoff, A., Venance, L., Blomstrand, F., and Giaume, C. (2002). Gap junctions and connexin expression in the normal and pathological central nervous system. Biol. Cell *94*, 457–475.

41. Poplawski, G., Ishikawa, T., Brifault, C., Lee-Kubli, C., Regestam, R., Henry, K.W., Shiga, Y., Kwon, H., Ohtori, S., Gonias, S.L., and Campana, W.M. (2018). Schwann cells regulate sensory neuron gene expression before and after peripheral nerve injury. Glia *66*, 1577–1590.

42. Zuchner, S. (2021). Schwann cell gene therapies in sight. Gene Ther. *28*, 618–619.

43. Negro, S., Pirazzini, M., and Rigoni, M. (2022). Models and methods to study Schwann cells. J. Anat. *241*, 1235–1258.

44. Gautier, B., Hajjar, H., Soares, S., Berthelot, J., Deck, M., Abbou, S., Campbell, G., Ceprian, M., Gonzalez, S., Fovet, C.M., et al. (2021). AAV2/9-mediated silencing of PMP22 prevents the development of pathological features in a rat model of Charcot-Marie-Tooth disease 1 A. Nat. Commun. *12*, 2356.

45. Stavrou, M., Kagiava, A., Choudury, S.G., Jennings, M.J., Wallace, L.M., Fowler, A.M., Heslegrave, A., Richter, J., Tryfonos, C., Christodoulou, C., et al. (2022). A translatable RNAi-driven gene therapy silences PMP22/Pmp22 genes and improves neuropathy in CMT1A mice. J. Clin. Investig. *132*, e159814.

46. Kagiava, A., Karaiskos, C., Richter, J., Tryfonos, C., Jennings, M.J., Heslegrave, A.J., Sargiannidou, I., Stavrou, M., Zetterberg, H., Reilly, M.M., et al. (2021). AAV9-mediated Schwann cell-targeted gene therapy rescues a model of demyelinating neuropathy. Gene Ther. *28*, 659–675.

47. LeBlanc, S.E., Jang, S.W., Ward, R.M., Wrabetz, L., and Svaren, J. (2006). Direct regulation of myelin protein zero expression by the Egr2 transactivator. J. Biol. Chem. *281*, 5453–5460.

48. Homs, J., Ariza, L., Pagès, G., Udina, E., Navarro, X., Chillón, M., and Bosch, A. (2011). Schwann cell targeting via intrasciatic injection of AAV8 as gene therapy strategy for peripheral nerve regeneration. Gene Ther. *18*, 622–630.

49. Zhuang, G.Z., Upadhyay, U., Tong, X., Kang, Y., Erasso, D.M., Fu, E.S., Sarantopoulos, K.D., Martin, E.R., Wiltshire, T., Diatchenko, L., et al. (2018). Human carbonic anhydrase-8 AAV8 gene therapy inhibits nerve growth factor signaling producing prolonged analgesia and anti-hyperalgesia in mice. Gene Ther. *25*, 297–311.

50. Kudo, M., Wupuer, S., Fujiwara, M., Saito, Y., Kubota, S., Inoue, K.I., Takada, M., and Seki, K. (2021). Specific gene expression in unmyelinated dorsal root ganglion neurons in nonhuman primates by intra-nerve injection of AAV 6 vector. Mol. Ther. Methods Clin. Dev. *23*, 11–22.

51. Towne, C., Raoul, C., Schneider, B.L., and Aebischer, P. (2008). Systemic AAV6 delivery mediating RNA interference against SOD1: neuromuscular transduction does not alter disease progression in fALS mice. Mol. Ther. *16*, 1018–1025.

52. Boutary, S., Caillaud, M., El Madani, M., Vallat, J.M., Loisel-Duwattez, J., Rouyer, A., Richard, L., Gracia, C., Urbinati, G., Desmaële, D., et al. (2021). Squalenoyl siRNA PMP22 nanoparticles are effective in treating mouse models of Charcot-Marie-Tooth disease type 1 A. Commun. Biol. *4*, 317.

53. Florio, F., Ferri, C., Scapin, C., Feltri, M.L., Wrabetz, L., and D'Antonio, M. (2018). Sustained Expression of Negative Regulators of Myelination Protects Schwann Cells from Dysmyelination in a Charcot-Marie-Tooth 1B Mouse Model. J. Neurosci. *38*, 4275–4287.

54. O'Carroll, S.J., Cook, W.H., and Young, D. (2020). AAV Targeting of Glial Cell Types in the Central and Peripheral Nervous System and Relevance to Human Gene Therapy. Front. Mol. Neurosci. *13*, 618020.

55. Tran, D.Q.H., Dugani, S., Pham, K., Al-Shaafi, A., and Finlayson, R.J. (2011). A randomized comparison between subepineural and conventional ultrasound-guided popliteal sciatic nerve block. Reg. Anesth. Pain Med. *36*, 548–552.

56. Jung Kim, H., and Hyun Park, S. (2014). Sciatic nerve injection injury. J. Int. Med. Res. *42*, 887–897.

57. Moayeri, N., and Groen, G.J. (2009). Differences in quantitative architecture of sciatic nerve may explain differences in potential vulnerability to nerve injury, onset time, and minimum effective anesthetic volume. Anesthesiology *111*, 1128–1134.

58. Glatzel, M., Flechsig, E., Navarro, B., Klein, M.A., Paterna, J.C., Büeler, H., and Aguzzi, A. (2000). Adenoviral and adeno-associated viral transfer of genes to the peripheral nervous system. Proc. Natl. Acad. Sci. USA *97*, 442–447.

59. Gonzalez, S., Fernando, R.N., Perrin-Tricaud, C., and Tricaud, N. (2014). In vivo introduction of transgenes into mouse sciatic nerve cells *in situ* using viral vectors. Nat. Protoc. *9*, 1160–1169.

60. Shin, S.M., Lauzadis, J., Itson-Zoske, B., Cai, Y., Fan, F., Natarajan, G.K., Kwok, W.M., Puopolo, M., Hogan, Q.H., and Yu, H. (2022). Targeting intrinsically disordered regions facilitates discovery of calcium channels 3.2 inhibitory peptides for adeno-associated virus-mediated peripheral analgesia. Pain *163*, 2466–2484.

61. Shin, S.M., Wang, F., Qiu, C., Itson-Zoske, B., Hogan, Q.H., and Yu, H. (2020). Sigma-1 receptor activity in primary sensory neurons is a critical driver of neuropathic pain. Gene Ther. *29*, 1–15.

62. Yu, H., Fischer, G., Ferhatovic, L., Fan, F., Light, A.R., Weihrauch, D., Sapunar, D., Nakai, H., Park, F., and Hogan, Q.H. (2013). Intraganglionic AAV6 results in efficient and long-term gene transfer to peripheral sensory nervous system in adult rats. PLoS One *8*, e61266.

63. Shin, S.M., Itson-Zoske, B., Cai, Y., Qiu, C., Pan, B., Stucky, C.L., Hogan, Q.H., and Yu, H. (2020). Satellite glial cells in sensory ganglia express functional transient receptor potential ankyrin 1 that is sensitized in neuropathic and inflammatory pain. Mol. Pain *16*, 1744806920925425.

64. Gemes, G., Bangaru, M.L.Y., Wu, H.E., Tang, Q., Weihrauch, D., Koopmeiners, A.S., Cruikshank, J.M., Kwok, W.M., and Hogan, Q.H. (2011). Store-operated Ca2+ entry in sensory neurons: functional role and the effect of painful nerve injury. J. Neurosci. *31*, 3536–3549.

65. Mikesell, A.R., Isaeva, O., Moehring, F., Sadler, K.E., Menzel, A.D., and Stucky, C.L. (2022). Keratinocyte PIEZO1 modulates cutaneous mechanosensation. Elife *11*, e65987.

66. Mi, D., Yuan, Y., Zhang, Y., Niu, J., Wang, Y., Yan, J., Yang, Y., and Hu, W. (2019). Injection of Fluoro-Gold into the tibial nerve leads to prolonged but reversible functional deficits in rats. Sci. Rep. *9*, 9906.

67. Hellman, A., Maietta, T., Byraju, K., Park, Y.L., Liss, A., Prabhala, T., Neubauer, P., Williams, E., Burdette, C., Shin, D.S., et al. (2020). Effects of external low intensity focused ultrasound on electrophysiological changes *in vivo* in a rodent model of common peroneal nerve injury. Neuroscience *429*, 264–272.

68. Chaplan, S.R., Bach, F.W., Pogrel, J.W., Chung, J.M., and Yaksh, T.L. (1994). Quantitative assessment of tactile allodynia in the rat paw. J. Neurosci. Methods *53*, 55–63.

69. Yu, H., Fischer, G., Jia, G., Reiser, J., Park, F., and Hogan, Q.H. (2011). Lentiviral gene transfer into the dorsal root ganglion of adult rats. Mol. Pain *7*, 63.